bioRxiv preprint doi: https://doi.org/10.1101/103937; this version posted April 5, 2017. The copyright holder for this preprint (which was not certified by peer review) is the author/funder. All rights reserved. No reuse allowed without permission.

Astral microtubule dynamics regulate anaphase oscillation onset and set a robust final position for the *Caenorhabditis elegans* zygote spindle

Hélène Bouvrais,[1,2,*] Laurent Chesneau,[1,2] Sylvain Pastezeur,[1,2] Marie Delattre,[3] and Jacques Pécréaux[1,2,*]

Affiliations

[1]CNRS UMR 6290, F-35043 Rennes, France.

[2]University of Rennes 1, UEB, SFR Biosit, School of Medicine, F-35043 Rennes, France

[3]Laboratory of Molecular Biology of the Cell, École Normale Supérieure de Lyon, CNRS, F-69364 Lyon, France

Correspondence: helene.bouvrais@univ-rennes1.fr; jacques.pecreaux@univ-rennes1.fr (Lead Contact)

bioRxiv preprint doi: https://doi.org/10.1101/103937; this version posted April 5, 2017. The copyright holder for this preprint (which was not certified by peer review) is the author/funder. All rights reserved. No reuse allowed without permission.

Graphical abstract

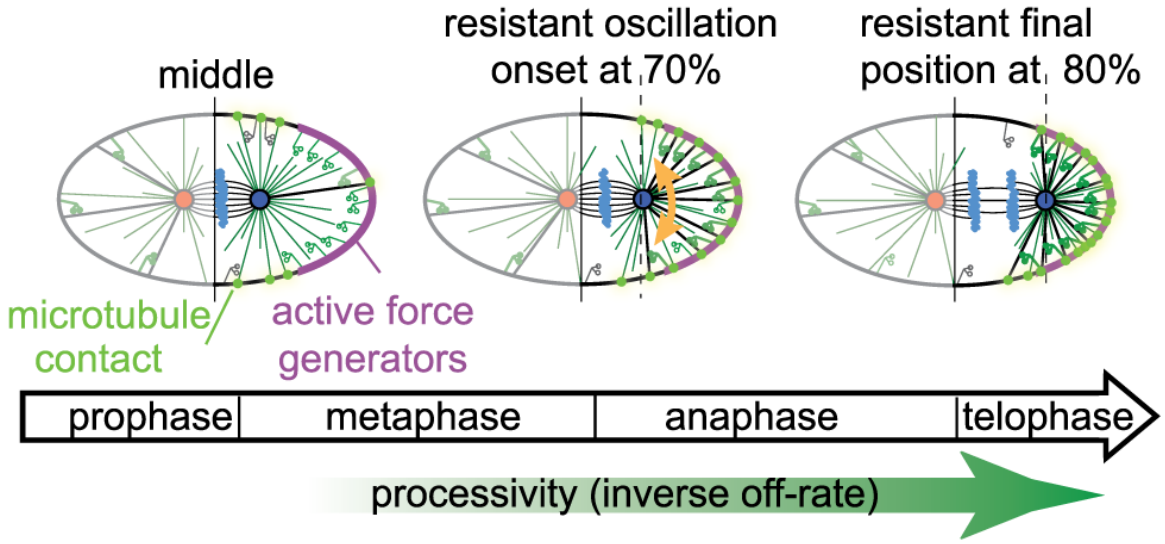

Abstract

Background: During asymmetric division of the *Caenorhabditis elegans* nematode zygote, the polarity cues distribution and daughter cell fates depend on the correct positioning of the mitotic spindle which results from both centering and cortical pulling forces. Revealed by spindle rocking, these pulling forces are regulated by the force generator dynamics, which are related to mitosis progression. This may be combined with a second regulation, this one by the posterior spindle pole position, which can be seen when comparing related species. **Results:** After delaying anaphase onset, we identified a positional pulling force regulation in *C. elegans*, which we ascribed to microtubule dynamics at the cortex. Indeed, in mapping the contacts we found a correlation between the centrosome–cortex distance and the microtubule contact density. This density in turn modulates pulling force generator activity. We expanded our model of spindle rocking and predicted then experimentally validated that the oscillation onset position resists changes in cellular geometry and number of force generators. Consistent with final spindle position measurements, this new model accounts for a lower dependence on force generator dynamics and quantities than predicted by the previous model. **Conclusion:** The spindle position regulates the rapid increase in forces needed for anaphase oscillation and positioning through the spatial modulation of microtubule-cortex contacts. This regulation superimposes that of force generator processivity, putatively linked to the cell cycle. This novel control confers resistance to variations in zygote geometry and dynamics of cortical force generators. Interestingly, this robustness originates in cell mechanics rather than biochemical networks.

Highlights

- Microtubule contacts at the cortex concentrate in regions close to the centrosomes.
- This regulates pulling forces and creates a positional switch on oscillation onset.
- The onset position resists changes in embryo length and force generator dynamics.
- The final centrosome position resists changes in generator quantities and dynamics.

bioRxiv preprint doi: https://doi.org/10.1101/103937; this version posted April 5, 2017. The copyright holder for this preprint (which was not certified by peer review) is the author/funder. All rights reserved. No reuse allowed without permission.

Asymmetric cell divisions, with their differing daughter cell sizes, contents, and fates, are essential to the development of multicellular organisms[1,2]. As with many other species[3,4], the mitotic spindle helps position the cytokinesis cleavage furrow in the nematode *Caenorhabditis elegans*[5]. To correspond to cortical polarity cues, the spindle needs to be oriented along the polarity axis[6] and displaced out of the cell centre before cytokinesis[6,7]. Most asymmetric division includes pulling forces from the cell cortex that are exerted on the astral microtubule plus ends, and these forces are key in positioning and orienting the spindle[6,7,8].

In the one-cell nematode embryo, cortical forces are generated by a well-conserved trimeric complex which pulls on astral microtubules. The complex is made up of a dynein/dynactin complex, a LIN-5 NuMA homolog, and the G-protein regulators GPR-1/2, which are mammalian LGN homologs[9]. In an asymmetric division, GPR-1/2 reflect polarity cues[10] through their asymmetric locations[11,12], increasing the number of local active force generators[10,13]. During the centring phase[14], GPR-1/2 help orient the spindle along the anteroposterior axis (AP axis). They also aid in "overcentration," the displacement of the pronuclei centrosome complex (PCC) from the posterior side of the embryo to a slightly anterior position[12,15]. During prometaphase and metaphase, the spindle is maintained in the middle by centring forces that are independent of GPR-1/2 and may be caused by microtubule pushing on the cell cortex[16]. GPR-1/2-dependent cortical pulling forces become dominant in late metaphase and anaphase, displacing the spindle posteriorly, rocking it, and contributing to its elongation[17,18,19].

The activity of the cortical force generators is regulated in three different ways. The first is in space, through variation in *active* force generator counts across the distinct cortical regions in response to polarity cues. Twice as many force generators are active in the posterior cortex, where the PAR-2 polarity protein is present, than in the anterior one[10,17,20]. However, this active region only goes from 70% of the AP axis to the posterior tip of the embryo. This is because the LET-99 protein inhibits the GPR-1/2 location in the middle region (40 to 70% of the AP axis)[21,22]. Secondly, the number of active force generators is regulated in time, as it increases during cell division[18], likely according to mitotic progression[23]. Spindle rocking and posterior displacement can be explained by an anaphase-wide decrease in the force generator microtubule off-rate, which results in an increase in the overall pulling force[19] (Supplementary Text 2.2.1). In a third type of regulation, microtubule dynamics can also regulate cortical pulling forces[24]. Our initial "tug-of-war" physical model assumed that astral microtubules were abundant at the cortex during anaphase, and that the only limiting factor was the binding/unbinding dynamics of the force generators. However, such an abundance of microtubules, likely to occur during anaphase, is questionable in earlier phases. Indeed, Kozlowski et al. proposed a model in which limited microtubule access to the cortex accounts for spindle oscillation[25]. In addition, the duration of microtubule contacts at the cell cortex appears to be different on the anterior and posterior sides of the embryo[24]. Thus microtubule dynamics could regulate in another way, increasing the number of active force generators along the course of the cell division[26].

Previous studies have emphasized the key role of microtubules in the positioning of the microtubule-organizing centre (MTOC). Indeed, they can "sense" cell geometry, for example to bring the MTOC to the cell centre[27,28], or to orient the nucleus by exerting pulling forces that scale with microtubule length[29]. Similarly, in HeLa cells, microtubules "integrate" the adhesive pattern, whose cues are cortical, to orient the spindle accordingly[30]. In the *C. elegans* embryo, microtubules may contribute the orientation of the spindle by combining oblong embryo shape with polarity cues[31]. We therefore wondered whether the different microtubule contact densities in various regions of the cortex would modulate cortical force generation.

We recently observed in *Caenorhabditis briggsae* that both anaphase spindle oscillation onset and thus pulling forces are controlled by the position of the posterior spindle pole rather than by mitosis progression. In fact, oscillations start when the posterior pole reaches 70% of the AP axis in two nematode species (*C. elegans* and *C. briggsae*) which diverged 100 million years ago. Interestingly, in *C. briggsae,* this position was reached 30 seconds after anaphase onset but simultaneously to this onset in *C. elegans*. Taking into account the fact that GPR-1/2 levels are key to the regulation of cortical pulling forces[10,17], this robust oscillation onset is even more striking, since GPR is duplicated in *C. elegans* and because the GPR sequences are different in the two species[12]. These observations suggest that a positional switch controls pulling forces, and we propose here that this switch has to do with microtubule dynamics.

bioRxiv preprint doi: https://doi.org/10.1101/103937; this version posted April 5, 2017. The copyright holder for this preprint (which was not certified by peer review) is the author/funder. All rights reserved. No reuse allowed without permission.

Measuring the residency time of microtubules at the cell cortex throughout mitosis was key to exploring our hypothesis. While the microtubule dynamics in the cytoplasm over time are quite clear in nematode embryos[26], the time spent at the cortex is less well understood, with published values ranging from 1 to more than 10 seconds[24,25]. This discrepancy can be explained by the accelerated dynamics of microtubules, which requires high frame rate imaging. In this paper, we carefully measured the spatial variation of such dynamics. We used the results to decipher the regulatory role of microtubule dynamics on cortical pulling forces, thus accounting for the decoupling between oscillation and anaphase onsets observed in *C. briggsae*[12] and in *C. elegans*. Our initial tug–of–war model, focused on force generator dynamics, was expanded to encompass this cortical pulling force positional switch. We challenged the new model, comparing the switch's predicted and experimental resistances to both embryo shape variation and displacing of the active force generator region boundaries. Investigating the posterior displacement and using an *in silico* approach, we explored the consequences of this novel regulation of the spindle's final position, which itself contributes to cleavage furrow positioning.

Results

Spindle oscillations can start before anaphase onset in *C. elegans*.

We previously reported that the position of the spindle's posterior pole controls the onset of spindle oscillation in *C. briggsae*[12]. We wondered whether the simultaneous onsets of anaphase and oscillation seen in *C. elegans* were coincidental. To explore this, we delayed anaphase using a *such-1*^{ANAPC5}*(h1960)* mutant of the anaphase-promoting complex/cyclosome (APC/C)[32], labelling centrosomes and chromosomes using SPD-2^{CEP192}::GFP;HIS-58^{H2B}::mcherry. We tracked the centrosomes[16,19], observing oscillations before anaphase started (Table 1). The oscillations started when the posterior centrosome was at 70% of embryo length in both the control and the mutant, as we observed previously in *C. briggsae*[12]. In contrast, for both strains the die-down of oscillation occurred about two minutes after anaphase onset, regardless of the anaphase timing, thus leading to different durations (Table 1). We concluded that a positional switch controls anaphase oscillation onset in *C. elegans* embryos, while their ending point depends on the cell cycle. This "centrosome-tracking" assay was instrumental in our functional testing of the positional switch.

Microtubule contacts at the cortex depend upon centrosomal positioning.

To account for this positional switch, we hypothesized that the network of astral microtubules emanating from the posterior centrosome would have reduced accessibility to the "active region," the posterior crescent of the cortex where the active force generators are located[22]. When the spindle is close to the cell's centre, the density of microtubule contacts in the active region would be very low. This density would then increase as the posterior centrosome is displaced toward the posterior. The oscillations build up once a threshold of active force generators is reached, and they would depend on the position of the centrosome. We tested this by directly measuring the spatial distribution of the microtubule contacts at the cortex ("landing" assay). We were able to preserve the embryo shapes by using spinning disk microscopy and by measuring microtubule dynamics using α-tubulin rather than EB labelling (Supplementary Experimental Procedures). Because the dynamics are so fast, we viewed the cortical contacts at a speed of 10 frames per second. Our method generated an exponential distribution of residency times (Supplementary Fig. S1B) consistent with previously published values[25]. We calculated the distribution of the microtubule contacts along the AP axis. To reduce uncertainty, we block–averaged the distribution in ten equivalent regions along the AP axis, and used a 10-second running average. We observed spatial heterogeneity with high-density ridge lines and an overall increase in contacts between metaphase and anaphase, consistent with the increasing nucleation rate previously described[26] (Supplementary Fig. S1C). To test whether the ridge lines corresponded to the centrosomal position, we used a wide-field microscope to view the spindle plane in the same strain and at the same temperature. We tracked the centrosomes as we have previously described[19]. We then combined the results from both experiments and aligned them with anaphase onset (Supplementary Experimental Procedures). We found that centrosome positioning coincides with the ridge lines (Fig. 1). We had initially observed the positional switch on cortical pulling forces in one-cell *C. briggsae* embryos[12], apparently related to the modulation of microtubule cortical contacts. So we performed the same experiments in this species, obtaining similar results (Supplementary Fig. S2). We concluded that the distance of the centrosome to the

bioRxiv preprint doi: https://doi.org/10.1101/103937; this version posted April 5, 2017. The copyright holder for this preprint (which was not certified by peer review) is the author/funder. All rights reserved. No reuse allowed without permission.

cortex strongly controls the number of microtubule end contacts in both species. As a consequence, the number of active region contacts increases with the posterior displacement of the spindle.

A comprehensive model for pulling force regulation and spindle oscillations

We expected that the modulation of microtubule contact density by the centrosome-to-cortex distance would regulate the cortical pulling forces and create the previously observed positional switch. Indeed, we have already reported on *C. briggsae* whose oscillations start 30 s after anaphase onset because of a delay in centrosome posterior displacement[12]. Here we observed (Table 1) that when the posterior centrosome is not far enough to the posterior, there are fewer microtubules at the cortex and not enough active force generators[19], thus preventing anaphase oscillation. Such a putative positional control of oscillation onset may seem to conflict with the initial tug-of-war hypothesis, which posits that both the build-up and die-down timings are regulated by the processivity of force generators[19], possibly related to mitosis progression[23]. We therefore expanded the initial model to quantitatively capture how the microtubule network could create a positional switch on cortical pulling forces.

Expanding the model to account for microtubule dynamics

We modelled the dynamic instability of microtubules, taking into account their alternating growth and shrinkage phases[33], but assuming that the force-dependence of the catastrophe rate is negligible[34]. We also assumed that catastrophes happen only at the cortex (no free end catastrophes), and that microtubules fully depolymerize upon shrinking (negligible rescue rates)[25,26,35] (Supplementary Text 2.1.1). We set a constant number of microtubule nucleation sites at the centrosomes, which were never empty[34], and the microtubules emanated from there in an isotropic angular distribution[26,36]. We computed the number of microtubules that reached the cortex in the active region (Fig. 2C, *left*, purple colour) as a function of the position of the posterior centrosome (Fig. 2A, black curve). This highlighted a steeper increase that starts at a point consistent with the onset of oscillation at 70% of embryo length. We modelled the embryo as an ellipsoid, but our result was independent of that hypothesis, as various superellipse based shapes[37] all yielded the same switch behaviour (Supplementary Fig. S3 and Text 2.1.3). We therefore continued modelling with an ellipsoid embryo shape. We concluded that microtubule dynamics can implement the experimentally observed positional switch by regulating the number of microtubules available to force generators. Furthermore, the large number of microtubules that reach the active region during mid and late anaphase is consistent with the previous tug-of-war model's assumption that microtubules saturate a limited number of cortical force generators during this period[19,38].

Accounting for force generator dynamics

Force generator dynamics set oscillation frequencies and determine peak amplitude and die-down timings[19]. To combine this regulation with the proposed control by microtubule dynamics, we modelled the binding of microtubules and force generators[9] as a first-order chemical reaction using the law of mass action, assuming no cooperative binding between force generators[39]. We estimated the association constant from the binding and unbinding rates used in the anaphase oscillation model (Supplementary Text 2.2.2)[19]. For the sake of clarity, we initially assumed a time-independent association constant for modelling the oscillation onset. This enabled us to compute the number of engaged force generators versus the posterior centrosome positions (Supplementary Text 2.2). We found that when the centrosome was far from the posterior tip, a scarcity of astral microtubule contacts in the active region of the cortex limited the number of engaged force generators to below the previously described oscillation threshold[19] (Fig. 2B, black line, and 2C, *left*). Upon posterior displacement of the centrosome past 60% of the AP axis, we observed a steep increase in engaged force generators, similar to the number of microtubule contacts (compare the black curves in Figure 2A and B). This was followed by a saturation starting from 70% of the AP axis. This switch-like behaviour is consistent with our positional switch hypothesis. The precise position at which oscillations started was dependent on the position of the active region boundary (Fig. 2B). We assumed that this region was set up by LET-99 force generator inhibition[22] and extended from 70 to 100% of the AP-axis[21] (see the experimental validation below). Thus, the positional switch is located at about 70% of the AP axis, consistent with our previous experiments, so we retained this position for the modelling and simulations which followed. The saturation of engaged force generators that we saw suggests that, during anaphase, the control parameter is their dynamics, not their quantity. This is coherent since oscillation peak and die-down timings are mostly independent of centrosome positioning but do occur after an anaphase onset delay (Table 1), as suggested by the initial model. In writing the law of mass action for the force generators, we assumed that the cell membrane cortical force

bioRxiv preprint doi: https://doi.org/10.1101/103937; this version posted April 5, 2017. The copyright holder for this preprint (which was not certified by peer review) is the author/funder. All rights reserved. No reuse allowed without permission.

generator anchors diffuse fast enough to not be limiting (Supplementary Text 2.2.4). We checked this assumption by computing the number of engaged force generators versus the position of the posterior centrosome. This was done under microtubule-force generator binding modelled by applying the law of mass action to areal concentrations, and we again found a positional switch (compare Supplementary Fig. S4A and B, black lines). In conclusion, our model suggests that oscillation onset is specifically regulated by the posterior displacement of the posterior centrosome via the dynamics of astral microtubules.

Microtubule and force generator dynamics set two independent switches

We next wondered how processivity of the force generators (reflecting mitosis progression[19,23]) and the posterior centrosome's position combine to initiate oscillation. We completed our expanded model by making the microtubule-force generator association constant dependent on time through the off-rate, which is the inverse of processivity. The off-rate was the control parameter in the initial model, and it decreases along the course of mitosis[19] (Supplementary Text 2.2.5). In contrast, in the new model the force generator on-rate is not constant, depending both on the number of microtubules available at the cortex for binding a force generator (Supplementary Text 2.2.2), and on polarity[13] (Supplementary Text 3). This suggests that to enable oscillation, the posterior centrosome needs to be close to the posterior tip of the embryo, which supports our positional switch experiment (Fig. 2D, blue curve). In addition to a positional control, the processivity needs to be in a given range (Fig. 2D, blue region): out of this zone, the oscillations are dampened (Fig. 2D, white areas). This is consistent with control via a steady increase in processivity[19], and leads to a dual control of the pulling forces. Interestingly, as seen experimentally (Supplementary Text 2.2.5), the posterior centrosome position more strongly influences oscillation onset than die-down (Fig. 2D, green and blue curves). To summarize, we expanded our initial tug-of-war model by adding a positional switch to control oscillation onset and thus the pulling forces that contribute to spindle elongation and posterior displacement.

We then decided to validate the model using three experiments. We first tested whether the boundary of the active region sets the centrosome position that corresponds to oscillation onset. We then confirmed that the onset is not controlled by force generator activity (Supplementary Text 2.2.3). And finally, we tested the positional switch prediction which said that it is the position rather than the timing of oscillation onset that weakly depends on embryo length.

The position of the active region boundary controls oscillation onset

In building the model, we reported that the position where oscillation starts is controlled by the boundary of the region where the active force generators are confined. Our model predicted that when this active region extends more anteriorly, the oscillation start position is also displaced anteriorly (Fig. 2B, blue and green curves). To check this, we increased the active region by partially depleting the protein LET-99 by RNAi, which is thought to restrict the force generator regulators GPR-1/2 to that area[11]. In treated embryos, the active force generators are thought to extend across the embryo's entire posterior half[22]. Indeed, we observed that as compared to the control, the position at which oscillations began was significantly displaced towards the anterior (Fig. 3A), in agreement with the model's predictions. Interestingly, the oscillations also started earlier with respect to anaphase onset, further supporting the idea that the oscillation onset is independent of mitosis progression (Fig. 3B). We concluded that the position of the active region boundary probably controls the position where oscillation onset will occur.

Because the positional switch relies on microtubule dynamics, our expanded model predicts that the position of oscillation onset will be independent of the total number of force generators (Supplementary Fig. S6A) when this count is above the threshold required for oscillations. We previously produced data that suggested such a result[12], and these experiments are reproducible (Supplementary Text 2.2.3).

The oscillation onset position is less sensitive to embryo size

Our expanded tug-of-war model suggested that the oscillation onset position only weakly depends upon the length of the embryo (Fig. 4A). To investigate this increased robustness as compared to the initial model, we depleted C27D9.1 and CID-1 by RNAi to respectively obtain longer and shorter embryos. In both cases, the embryos were viable and showed no other visible phenotypes. We measured the variations in the timing and positioning of oscillation onset with respect to the variations in embryo length. For both cases, we fitted a linear model, measuring oscillation onset timing slopes 10 times larger than that of the

bioRxiv preprint doi: https://doi.org/10.1101/103937; this version posted April 5, 2017. The copyright holder for this preprint (which was not certified by peer review) is the author/funder. All rights reserved. No reuse allowed without permission.

oscillation onset position (Fig. 4B-C). This further suggests that the positioning and timing of oscillation initiation are not correlated to anaphase onset. This is also perfectly consistent with the model's prediction that oscillation onset positions are less sensitive to embryo lengths (Fig. 4A). In contrast, embryo length does impact the point at which oscillation die-down begins (Fig. 4D), which is not a surprise since it is temporally controlled. We therefore concluded that these experiments validated the expanded tug-of-war model.

Sensitivity analysis of the oscillation onset positions using the new model

Using our expanded model, we performed a thorough sensitivity analysis (Supplementary Fig. S5). As expected, the microtubule counts (Supplementary Fig. S5F) and dynamics (Supplementary Fig. S5C) were critical for setting the position of oscillation onset. The embryo widths (Supplementary Fig. S5D) and proportional scaling (Supplementary Fig. S5E) were also influential, although to a lesser extent. Interestingly, as suggested by the robustness of the position of oscillation onset versus the embryo length (Fig. 4A), when the area is constant, the eccentricity has a reduced impact (Supplementary Fig. S5B). Similarly, the quantity (Supplementary Fig. S6A) and dynamics (Supplementary Fig. S4A) of the force generators appear to have only a small effect when they reach the oscillation threshold, as previously reported[19]. The cortical distribution of the force generators and their restriction to the active region are also key (Fig. 2B). In conclusion, the positional control of oscillation onset relies on microtubule dynamics, while mitosis progression control is performed through force generator processivity.

Astral microtubule dynamics regulate the final spindle position

Microtubule dynamics create feedback on the cortical pulling forces which set the spindle's final position.

Cortical pulling forces cause anaphase spindle oscillations, along with the posterior displacement of the spindle during late metaphase and anaphase[18,19]. In our initial model, we suggested that the final posterior centrosome position results from a balance between the cortical pulling forces and centring forces, which were modelled by a spring[19]. In contrast, in the improved model, the average number of engaged force generators depends not only on their dynamics but also on microtubule availability at the cortex, and thus centrosome positioning. We figured that the positional control of the pulling force generators causes a feedback loop on the final position of the spindle, which these forces contribute to setting. To investigate this hypothesis, we simulated posterior displacement using our expanded model with the TR-BDF2 algorithm[40] (Supplementary Text 3.1). To ensure the proper force balance on the spindle, we also included the anterior centrosome in the model by using a 0 to 40% active region corresponding to the area lacking LET-99[21]. However, we restricted the anterior centrosome to a fixed position. Furthermore, since the model is linearized it is limited to considering modest variations in parameters around their nominal values. On the anterior side, we used a two-fold lower force generator on-rate[13], which results in half the number of active force generators as found at the posterior[17]. We assumed that force applied to posterior centrosome and originated in anterior side is halved after anaphase onset because sister-chromatids separated. Finally, we modelled the centring force with a spring (according to [16]), using processivity to control the progression of mitosis[19]. We could reproduce the global kinematics of posterior displacement[16]: slow prior to anaphase, then accelerating afterward (Fig. 5, black curve, and Supplementary Fig. S7A5). In particular, the model accounts well for the final position of the posterior centrosome. On this basis, we aimed to test the model incorporating microtubule dynamics to explore the consequences of this inclusion on final spindle positioning.

The active region but not the total force generator count determines the final position of the spindle.

Consistent with observations in *let-99(RNAi)*-treated embryos (Fig. 3A),[22] the final position of the posterior centrosome was displaced anteriorly when the boundary of the posterior active crescent moved anteriorly, so long as the region was large enough to initiate posterior displacement in the first place (Supplementary Fig. S7B). This result differs from the initial model's prediction that under similar cortical forces, the posterior displacement would be the same[22]. The asymmetry in cortical pulling forces that cause the posterior displacement is due to a larger number of active force generators on the posterior side[17]. This was initially assumed to reflect an asymmetric total number of generators, and was recently proposed to be due to an asymmetric distribution of GPR-1/2, leading to an asymmetric binding rate of force generators to microtubules (on-rate)[13]. The initial model predicted a linear dependence between the number of active force generators and the final spindle position[16]. Our expanded model is less sensitive to

bioRxiv preprint doi: https://doi.org/10.1101/103937; this version posted April 5, 2017. The copyright holder for this preprint (which was not certified by peer review) is the author/funder. All rights reserved. No reuse allowed without permission.

that count (Supplementary Fig. S7CD and Supplementary Text 2.2.3), which is consistent with the observed robustness of oscillation onset positioning (Supplementary Fig. S6C). This robustness is attributed to a smaller increase in cortical pulling forces when the centrosome moves further to the posterior after crossing the boundary position (Supplementary Fig. S7A4). In conclusion, the final spindle position's dependence on the cortical boundary rather than the number of active force generators present suggests that the initial tug-of-war model is not enough to correctly understand the mechanism of spindle final position determination, and that the microtubule dynamics also have to be considered.

The final spindle position is resistant to changes in the final force generator processivity.

In the initial model, the final spindle position was predicted to not only depend on the imbalance of force generator quantities or their on-rates, but also on their final processivity. This prediction does not reflect *such-1* mutant results. This mutation results in altered mitosis progression and thus probably altered final processivity but normal final posterior centrosomal positioning (Table 1)[23]. In contrast and in cases of moderate final processivity variations, our expanded model can account for this robustness (Fig. 5). The new model better explains the final spindle position's resilience in the face of changes in force generator quantities or dynamics, and this is particularly important since it is essential to the proper positioning of the cleavage furrow.

Discussion

In measuring the spatial distribution of microtubule contacts at the cell cortex, we found that it is uneven in space, concentrating more in the regions closer to the centrosomes. It is however noteworthy that due to the increased nucleation and persistence of microtubules, the total number of contacts scales up (Fig. 1, 80 s after anaphase onset), as expected from their regulation along the course of mitosis[26]. This contact distribution regulates the forces responsible not only for the anaphase spindle oscillations, but also for the spindle's posterior displacement. Interestingly, these causative forces are controlled by the positioning of the posterior centrosome, the so-called *positional switch*. The forces also contribute to spindle elongation, and their positional regulation might be linked to tension-based spindle assembly checkpoint satisfaction[41]. We expanded our tug-of-war spindle oscillation and posterior displacement model[19] to account for this, and validated it experimentally. In particular, we observed that the position of oscillation onset, but not the timing, is resistant to variations in embryo length. It is also correlated to the size of the posterior active force generator region, assumed to be limited by LET-99[21,22]. In the early stages of mitosis, the spindle lies in the middle of the embryo, and both of the centrosomes are far from their respective cortex. Therefore, the imbalance in active force generator quantities[17] causes a slight posterior pulling force, resulting in a slow posterior displacement[18] (Fig. 2C, *left*). The closer the posterior centrosome gets to the cortex, the larger the force imbalance becomes. This is because more microtubules reach the cortex, thus the pulling force builds up more rapidly, accelerating the posterior displacement. The number of engaged force generators increases, exceeding the threshold for oscillation onset[19] (Fig. 2C, *middle*). The pulling forces displacing the spindle start saturating, both because of the limited cortical anchors[19,42] and because once the posterior centrosome crosses the boundary of the active region, only the forces projected along the anteroposterior axis contribute to the spindle displacement (Supplementary Fig. S2C, *right*). Because they are opposing, these and the centring forces balance[19], setting the spindle's position at the end of mitosis.

This positional switch adds to the previously described temporal control by force generator processivity[19], which in turn reflects mitosis progression[23]. These two controls act independently, as they relate to two independent components: the *positional control* is determined by microtubule dynamics; and the *temporal control* is set by the force generator dynamics. Indeed, the curve reflecting the engaged force generator count versus the centrosome positioning (Fig. 2B) steeply increases starting at 60% of embryo length because of microtubule dynamics, while force generator dynamics cause the count to saturate above 70%. Our model suggests that there are two conditions necessary for oscillation onset (Fig. 2D, blue curve): enough microtubules in contact with the cortex's active region; and a force generator processivity that is high enough. Indeed, during anaphase, the temporal evolution of the cortical pulling force amplitudes is controlled by the force generator dynamics, as proposed previously and as indicated by the oscillation die-down timing[19]. This dual control of pulling forces was further confirmed by three experiments. First, we tested embryos treated with *let-99(RNAi)*. Their positional control is disturbed by anterior displacement of the active region boundary, and as predicted by the model (Supplementary Fig. S7B), the final centrosomal

bioRxiv preprint doi: https://doi.org/10.1101/103937; this version posted April 5, 2017. The copyright holder for this preprint (which was not certified by peer review) is the author/funder. All rights reserved. No reuse allowed without permission.

position is strongly altered (Fig. 3A) although the oscillation die-down timing is not significantly different than for the control (Fig. 3B). A second experiment was done in *such-1(h1960)* mutants, where temporal control is altered by a delay in anaphase onset. In this case, the time between anaphase onset and oscillation die-down was the same as in the control, implying that they were delayed in the same proportion. In contrast, the oscillation onset and die-down positions were not altered by a delayed anaphase onset (Table 1). Finally, when we used a *gpr-2* mutant to decrease the number of active force generators, we observed a precocious oscillation die-down (Supplementary Fig. S6B). The force generator quantity exceeded the threshold during a shorter time period, consistent with the initial model's prediction (see e.g. Figure 5C in [19]). Overall, these experiments support the conclusion that force generator dynamics dominate the control of anaphase oscillations after their onset.

We hypothesized that these combined controls, in particular the proposed positional switch, confer some robustness to the final position of the posterior centrosome and consequently of the spindle. This may be due to buffering against variations in the initial centrosomal positions (Supplementary Fig. S7E), or may be caused by the final processivity, which determines the final cortical pulling forces (Fig. 5). In terms of asymmetric cell division, the final spindle position contributes to fixing the cytokinesis cleavage furrow position, essential for the correct distribution of cell polarity cues and thus daughter cell fates[1,2,5]. In addition to studying the *C. elegans* nematode alone, we also recently performed a comparative study between two nematode cousins (*C. elegans* and *C. briggsae*)[12]. We found that cortical force generator regulation is altered because there is a duplication in *C. elegans* (GPR-1 and GPR-2) while *C. briggsae* only displays GPR-2[12]. We proposed that this evolution was made possible by the positional switch and the resulting resistance to force generator quantity and dynamics. Indeed, *C. briggsae* microtubule contacts at the cell cortex are distributed as they are in *C. elegans* (Supplementary Fig. S3), and resistance to embryo length variations is also observed[12]. Interestingly, the positional control of anaphase oscillation onset in *C. briggsae* results in a 30 s delay between oscillation and anaphase onsets (attributed to spindle "overcentration"[12]), while the oscillation die-down is synchronous with anaphase onset as predicted by our model. Furthermore, cross-species insertion of GPR genes modulates oscillation amplitude but preserves the positional switch, which is consistent with our *gpr-2(ok1179)* experiment. The robustness of final spindle positioning is likely to be true in more than just these two species[43]. During the course of evolution, the proposed robustness mechanism has enabled changes in the regulation of nuclei/centrosome complex position, even though the regulation is essential.

The dynamic instability of microtubules is at the core of this robustness mechanism. More precisely, it relies on the number of microtubule cortical contacts, which reflects the distance between the centrosome and the cortex. Indeed, said distance is measured in "units of microtubule dynamics" (Supplementary Text 2.1.2). This is a classic mechanism for creating centring[28,44] or other shape-dependent mechanisms[29,45,46], although it was always inferred from cell-level properties. In contrast, the distribution of the microtubule end contacts located at the cortex was obtained from microscopic measurements. We observed a density ratio of about 2 between the regions with the most and least microtubule contacts at a given time, and this ratio represents the sensitivity to centrosomal position (Supplementary Text 2.1.2). From a theoretical point of view, considering the ellipsoidal shape of the *C. elegans* embryo and the microtubule dynamics measurements (see above), the predicted maximal ratio is 1.64. Our experimental result is close to this prediction, suggesting that the microtubule dynamics parameters are optimal for the positional control we discuss here.

Conclusion

The study of the mechanism leading to the precise timing and positioning of the transverse oscillation onset in the *C. elegans* embryo has highlighted the key role of microtubule dynamics in probing the boundary of the active force generator region. This *positional control* of spindle rocking acts in addition to previously described regulation via pulling force machinery dynamics (*temporal control*). Both controls set independent switches to prevent premature force bursts. The finding of this supplementary positional control paves the way to understanding a novel mitosis choreography mechanism, going further than regulation by just the cell cycle.

bioRxiv preprint doi: https://doi.org/10.1101/103937; this version posted April 5, 2017. The copyright holder for this preprint (which was not certified by peer review) is the author/funder. All rights reserved. No reuse allowed without permission.

At anaphase, the positional control we report on here prevents the application of strong forces to the spindle before it reaches the point at which it normally elongates. We suggest that this control contributes to ensuring the correct positioning of cytokinesis cleavage furrow assembly. Indeed, this is positioned by two independent signals[47]. The first is the central spindle at the position where the spindle reaches its full elongation[48]. This elongation in turn requires cortical pulling forces[10], the regulation of which we investigated here. Therefore, the positional control of anaphase force bursts guarantees that the central spindle-signalling of the cleavage furrow will occur in the correct position.

At telophase, the cleavage furrow position is signalled by the spindle poles[49]. Interestingly, our proposed positional switch controls the final centrosome positions, since the forces that displace them are due to the same generators as spindle rocking and elongation. The mechanism ensures that the posterior centrosome has a robust final position that is scaled with the AP axis. Overall, the positional switch confers robustness to both signals that set the cleavage furrow position, therefore guaranteeing proper polarity cue distribution and the correct daughter cell fates[6,7]. We previously proposed that such a mechanism buffered changes in cortical pulling force levels and timings between the *C. elegans* and *C. briggsae* nematodes. This permitted substantial modifications in the essential GPR-1/2^{LGN} genes, which are part of the complex that generates cortical pulling forces[12].

Finally, the observed positional switch is caused by astral microtubules. They provide feedback about the posterior centrosome position to the cortical pulling forces which cause spindle displacement and rocking. This finding is a novel example of a microfilament-based system that controls essential aspects of cell division, such as cleavage furrow positioning and the granting of resistance to perturbation. In contrast with robustness resulting from classic biochemical signalling pathways[50,51], this mechanism is based solely on cell mechanics and component dynamics.

Material and Methods

Culturing C. elegans

C. elegans nematodes were cultured as described in [52], and dissected to obtain embryos. The strains were maintained at 25°C and imaged at 23°C, with the exception of the *gpr-2* mutant, *such-1* mutant, and their controls, which were maintained at 15°C and imaged at 18°C. The strains were handled on nematode medium plates and fed with OP50 bacteria.

Strains

TH65 *C. elegans* (*Ce*) YFP::TBA-2 (α-tubulin)[26] and ANA020 *C. briggsae* (*Cb*) GFP::β-tubulin strains with a microtubule fluorescent labelling were used as the controls for the "landing" assay. TH27 *C. elegans* GFP::TBG-1 (γ-tubulin)[53] and *C. briggsae* ANA022 TBG-1::GFP strains[12] displaying a centrosomal fluorescent labelling were the standards for the "centrosome-tracking" assay. For event timing, the control was the *C. elegans* TH231 (SPD-2::GFP) strain with centrosome labelling crossed to OD56 (mCherry::HIS-58) histone labelling (Table 1). It was crossed with the KR4012 *such-1(h1960)* mutant strain[32] to create JEP16. Centrosome tracking upon mutating *gpr-2* was performed on the JEP14 strain, which was obtained by crossing the 10x backcrossed strain TH291 *gpr-2*(*ok1179*) and TH27 *C. elegans* GFP::TBG-1 (γ -tubulin).

Gene inactivation through mutants or protein depletion by RNAi feeding

RNAi experiments were performed by ingestion of transformed HT115 bacteria. *let-99*, *cid-1* and *c27d9.1* genes were amplified from AF16 genomic ADN and cloned into the L4440 plasmid. To obtain stronger phenotypes, the feeding was performed at 20°C for 48h (except for *let-99*, which was only done for 16-24h). The control embryos for the RNAi experiments were treated with bacteria carrying the empty plasmid L4440.

Preparation of the embryos for imaging

Embryos were dissected in M9 buffer and mounted on a pad (2% w/v agarose, 0.6% w/v NaCl, 4% w/v sucrose) between a slide and a coverslip. Depending on the assay, they were observed using different microscopic setups. To confirm the absence of phototoxicity and photodamage, we checked for normal rates of subsequent divisions[54]. Fluorescent lines were imaged at 23°C unless otherwise indicated.

Imaging of microtubule contacts at the cortex ("landing" assay)

bioRxiv preprint doi: https://doi.org/10.1101/103937; this version posted April 5, 2017. The copyright holder for this preprint (which was not certified by peer review) is the author/funder. All rights reserved. No reuse allowed without permission.

We imaged *C. elegans* or *C. briggsae* one-cell embryos at the cortex plane in contact with the glass slide (Supplementary Fig. S1A), viewing from the nuclear envelope breakdown (NEBD) until the end of cell division. We did our utmost to preserve the embryo shapes. The thickness of the perivitelline space[55] therefore meant we had to use spinning disk microscopy rather than TIRF (Supplementary Fig. S1A). Cortical microtubule contact tracking was thus performed on a LEICA DMI6000 / Yokogawa CSU-X1 M1 spinning disc microscope, using a HCX Plan Apo 100x/1.4 NA oil objective. Illumination was performed using a white-light Fianium laser filtered around 514 nm in a homemade setup. To account for the fast speed of microtubule dynamics at the cortex, images were acquired at an exposure time of 100 ms (10 Hz) using an ultra-sensitive Roper Evolve EMCCD camera and the MetaMorph software (Molecular Devices) without binning. During the experiments, the embryos were kept at 23°C. To image embryos at the cortex, we typically moved the focus to 12 to 15 μm below the spindle plane (Supplementary Fig. S1A).

Centrosome imaging

For the "centrosome-tracking" and the "event-timing" assays, embryos were observed at the midplane using a Zeiss Axio Imager upright microscope modified for long-term time-lapse. First, an extra anti-heat filter was added to the mercury lamp light path. Secondly, to decrease the bleaching and obtain optimal excitation, we used an enhanced transmission 12 nm band pass excitation filter centred on 485 nm (AHF analysentechnik). We used a 100x/1.45 NA Oil plan-Apo objective. Images were acquired with an Andor iXon3 EMCCD 512x512 camera at 33 frames per second and using their Solis software. The beginning of the spindle's abrupt elongation (Supplementary Fig. S8A) was used as the marker for anaphase onset[16], and the centrosome tracks of individual embryos were aligned with this for averaging purposes or for overlay on the "landing" assay.

Statistics

Averaged values were compared using the two-tailed Student's *t*-test with correction for unequal variance except where otherwise stated. For the sake of simplicity, we recorded confidence levels using stars (*, $p \leq 0.05$; **, $p \leq 0.005$; ***, $p \leq 0.0005$; ****, $p \leq 0.00005$) and n.s. (non-significant, $p > 0.05$; sometimes omitted to save room). We abbreviated standard deviation by SD, standard error by s.e., and standard error of the mean by s.e.m.

Data processing, modelling, and simulation

All data analysis was developed using Matlab (The MathWorks). Modelling was performed using Wolfram Mathematica formal calculus software. Numerical simulations were performed using Matlab and Simulink (The MathWorks).

bioRxiv preprint doi: https://doi.org/10.1101/103937; this version posted April 5, 2017. The copyright holder for this preprint (which was not certified by peer review) is the author/funder. All rights reserved. No reuse allowed without permission.

References

1. Betschinger J, Knoblich JA. Dare to be different: asymmetric cell division in Drosophila, C. elegans and vertebrates. *Curr Biol* **14**, R674-685 (2004).

2. Gillies TE, Cabernard C. Cell division orientation in animals. *Curr Biol* **21**, R599-609 (2011).

3. Rappaport R. Cytokinesis in animal cells. *Int Rev Cytol* **31**, 169-213 (1971).

4. Knoblich JA. Asymmetric cell division: recent developments and their implications for tumour biology. *Nat Rev Mol Cell Biol* **11**, 849-860 (2010).

5. White EA, Glotzer M. Centralspindlin: At the heart of cytokinesis. *Cytoskeleton (Hoboken)* **69**, 882-892 (2012).

6. Morin X, Bellaiche Y. Mitotic spindle orientation in asymmetric and symmetric cell divisions during animal development. *Dev Cell* **21**, 102-119 (2011).

7. Gonczy P. Mechanisms of asymmetric cell division: flies and worms pave the way. *Nat Rev Mol Cell Biol* **9**, 355-366 (2008).

8. McNally FJ. Mechanisms of spindle positioning. *J Cell Biol* **200**, 131-140 (2013).

9. Nguyen-Ngoc T, Afshar, K., and Gonczy, P. Coupling of cortical dynein and G alpha proteins mediates spindle positioning in Caenorhabditis elegans. Nat. Cell Biol. *9* **1294-1302**, (2007).

10. Colombo K, Grill SW, Kimple RJ, Willard FS, Siderovski DP, Gonczy P. Translation of polarity cues into asymmetric spindle positioning in Caenorhabditis elegans embryos. *Science* **300**, 1957-1961 (2003).

11. Park DH, Rose LS. Dynamic localization of LIN-5 and GPR-1/2 to cortical force generation domains during spindle positioning. *Dev Biol* **315**, 42-54 (2008).

12. Riche S, Zouak M, Argoul F, Arneodo A, Pecreaux J, Delattre M. Evolutionary comparisons reveal a positional switch for spindle pole oscillations in Caenorhabditis embryos. *J Cell Biol* **201**, 653-662 (2013).

13. Rodriguez Garcia R, Chesneau L, Pastezeur S, Roul J, Tramier M, Pecreaux J. Dynamics of dynein at microtubule plus-ends and the cortex during the division of the C. elegans zygote. *bioRxiv preprint*, 118604 (2017).

14. Ahringer J. Control of cell polarity and mitotic spindle positioning in animal cells. *Curr Opin Cell Biol* **15**, 73-81 (2003).

15. Kimura A, Onami S. Local cortical pulling-force repression switches centrosomal centration and posterior displacement in C. elegans. *J Cell Biol* **179**, 1347-1354 (2007).

bioRxiv preprint doi: https://doi.org/10.1101/103937; this version posted April 5, 2017. The copyright holder for this preprint (which was not certified by peer review) is the author/funder. All rights reserved. No reuse allowed without permission.

16. Pecreaux J, *et al.* The Mitotic Spindle in the One-Cell C. elegans Embryo Is Positioned with High Precision and Stability. *Biophys J* **111**, 1773-1784 (2016).

17. Grill SW, Howard J, Schaffer E, Stelzer EH, Hyman AA. The distribution of active force generators controls mitotic spindle position. *Science* **301**, 518-521 (2003).

18. Labbe JC, McCarthy EK, Goldstein B. The forces that position a mitotic spindle asymmetrically are tethered until after the time of spindle assembly. *J Cell Biol* **167**, 245-256 (2004).

19. Pecreaux J, *et al.* Spindle oscillations during asymmetric cell division require a threshold number of active cortical force generators. *Curr Biol* **16**, 2111-2122 (2006).

20. Grill SW, Gonczy P, Stelzer EH, Hyman AA. Polarity controls forces governing asymmetric spindle positioning in the Caenorhabditis elegans embryo. *Nature* **409**, 630-633 (2001).

21. Wu JC, Rose LS. PAR-3 and PAR-1 inhibit LET-99 localization to generate a cortical band important for spindle positioning in Caenorhabditis elegans embryos. *Mol Biol Cell* **18**, 4470-4482 (2007).

22. Krueger LE, Wu JC, Tsou MF, Rose LS. LET-99 inhibits lateral posterior pulling forces during asymmetric spindle elongation in C. elegans embryos. *J Cell Biol* **189**, 481-495 (2010).

23. McCarthy Campbell EK, Werts AD, Goldstein B. A cell cycle timer for asymmetric spindle positioning. *PLoS Biol* **7**, e1000088 (2009).

24. Labbe JC, Maddox PS, Salmon ED, Goldstein B. PAR proteins regulate microtubule dynamics at the cell cortex in C. elegans. *Curr Biol* **13**, 707-714 (2003).

25. Kozlowski C, Srayko M, Nedelec F. Cortical microtubule contacts position the spindle in C. elegans embryos. *Cell* **129**, 499-510 (2007).

26. Srayko M, Kaya A, Stamford J, Hyman AA. Identification and characterization of factors required for microtubule growth and nucleation in the early C. elegans embryo. *Dev Cell* **9**, 223-236 (2005).

27. Dogterom M, Yurke B. Microtubule dynamics and the positioning of microtubule organizing centers. *Physical Review Letters* **81**, 485-488 (1998).

28. Dogterom M, Kerssemakers JW, Romet-Lemonne G, Janson ME. Force generation by dynamic microtubules. *Curr Opin Cell Biol* **17**, 67-74 (2005).

29. Minc N, Burgess D, Chang F. Influence of cell geometry on division-plane positioning. *Cell* **144**, 414-426 (2011).

30. Thery M, Jimenez-Dalmaroni A, Racine V, Bornens M, Julicher F. Experimental and theoretical study of mitotic spindle orientation. *Nature* **447**, 493-496 (2007).

bioRxiv preprint doi: https://doi.org/10.1101/103937; this version posted April 5, 2017. The copyright holder for this preprint (which was not certified by peer review) is the author/funder. All rights reserved. No reuse allowed without permission.

31. Tsou MF, Ku W, Hayashi A, Rose LS. PAR-dependent and geometry-dependent mechanisms of spindle positioning. *J Cell Biol* **160**, 845-855 (2003).

32. Tarailo M, Kitagawa R, Rose AM. Suppressors of spindle checkpoint defect (such) mutants identify new mdf-1/MAD1 interactors in Caenorhabditis elegans. *Genetics* **175**, 1665-1679 (2007).

33. Mitchison T, Kirschner M. Dynamic instability of microtubule growth. *Nature* **312**, 237-242 (1984).

34. Howard J. Elastic and damping forces generated by confined arrays of dynamic microtubules. *Phys Biol* **3**, 54-66 (2006).

35. O'Rourke SM, Christensen SN, Bowerman B. Caenorhabditis elegans EFA-6 limits microtubule growth at the cell cortex. *Nat Cell Biol* **12**, 1235-1241 (2010).

36. O'Toole ET, McDonald KL, Mantler J, McIntosh JR, Hyman AA, Muller-Reichert T. Morphologically distinct microtubule ends in the mitotic centrosome of Caenorhabditis elegans. *J Cell Biol* **163**, 451-456 (2003).

37. Edwards J. *An elementary treatise on the differential calculus, with applications and numerous examples*. Macmillan (1892).

38. Grill SW, Kruse K, Julicher F. Theory of mitotic spindle oscillations. *Physical Review Letters* **94**, 108104 (2005).

39. Koonce MP, Tikhonenko I. Dynein Motor Mechanisms. In: *Dyneins : structure, biology and disease* (ed^(eds King SM). 1st edn. Academic Press (2012).

40. Hosea ME, Shampine LF. Analysis and implementation of TR-BDF2. *Applied Numerical Mathematics* **20**, 21-37 (1996).

41. Cimini D, Wan X, Hirel CB, Salmon ED. Aurora kinase promotes turnover of kinetochore microtubules to reduce chromosome segregation errors. *Curr Biol* **16**, 1711-1718 (2006).

42. Grill SW, Hyman AA. Spindle positioning by cortical pulling forces. *Dev Cell* **8**, 461-465 (2005).

43. Farhadifar R*, et al.* Scaling, selection, and evolutionary dynamics of the mitotic spindle. *Curr Biol* **25**, 732-740 (2015).

44. Wuhr M, Dumont S, Groen AC, Needleman DJ, Mitchison TJ. How does a millimeter-sized cell find its center? *Cell Cycle* **8**, 1115-1121 (2009).

45. Daga RR, Nurse P. Interphase microtubule bundles use global cell shape to guide spindle alignment in fission yeast. *J Cell Sci* **121**, 1973-1980 (2008).

46. Thery M. Micropatterning as a tool to decipher cell morphogenesis and functions. *J Cell Sci* **123**, 4201-4213 (2010).

bioRxiv preprint doi: https://doi.org/10.1101/103937; this version posted April 5, 2017. The copyright holder for this preprint (which was not certified by peer review) is the author/funder. All rights reserved. No reuse allowed without permission.

47. Bringmann H, Hyman AA. A cytokinesis furrow is positioned by two consecutive signals. *Nature* **436**, 731-734 (2005).

48. Lewellyn L, Dumont J, Desai A, Oegema K. Analyzing the effects of delaying aster separation on furrow formation during cytokinesis in the Caenorhabditis elegans embryo. *Mol Biol Cell* **21**, 50-62 (2010).

49. Bringmann H, Cowan CR, Kong J, Hyman AA. LET-99, GOA-1/GPA-16, and GPR-1/2 are required for aster-positioned cytokinesis. *Curr Biol* **17**, 185-191 (2007).

50. McIntosh JR, Molodtsov MI, Ataullakhanov FI. Biophysics of mitosis. *Quarterly reviews of biophysics* **45**, 147-207 (2012).

51. Musacchio A. Spindle assembly checkpoint: the third decade. *Philos Trans R Soc Lond B Biol Sci* **366**, 3595-3604 (2011).

52. Brenner S. The genetics of Caenorhabditis elegans. *Genetics* **77**, 71-94 (1974).

53. Oegema K, Desai A, Rybina S, Kirkham M, Hyman AA. Functional analysis of kinetochore assembly in Caenorhabditis elegans. *The Journal of Cell Biology* **153**, 1209-1226 (2001).

54. Riddle DL. *C. elegans II*. Cold Spring Harbor Laboratory Press (1997).

55. Olson SK, Greenan G, Desai A, Muller-Reichert T, Oegema K. Hierarchical assembly of the eggshell and permeability barrier in C. elegans. *J Cell Biol* **198**, 731-748 (2012).

bioRxiv preprint doi: https://doi.org/10.1101/103937; this version posted April 5, 2017. The copyright holder for this preprint (which was not certified by peer review) is the author/funder. All rights reserved. No reuse allowed without permission.

Acknowledgments

The 10 times backcrossed strain *gpr-2(ok1179)* was a kind gift from Prof. Anthony A. Hyman. We thank Dr Grégoire Michaux for the feeding clone library and technical support. We also thank Drs Benjamin Mercat, Anne Pacquelet, Xavier Pinson, Yann Le Cunff, Danielle Fairbrass, Grégoire Michaux, Roland Le Borgne, Sébastien Huet, Marc Tramier, Claude Prigent, Françoise Argoul, and Alain Arnéodo for technical help, critical comments on the manuscript, and discussions about the project. JP was supported by a CNRS ATIP starting grant and *La ligue nationale contre le cancer*. Some strains were provided by the CGC, which is funded by NIH Office of Research Infrastructure Programs (P40 OD010440; University of Minnesota, USA). Microscopy imaging was performed at the MRIC facility, UMS 3480 CNRS / US 18 INSERM / University of Rennes 1. Spinning disk microscope was co-funded by the CNRS, *Rennes Métropole* and *Region Bretagne* (AniDyn-MT grant). HB's postdoctoral fellowship was funded by *Region Bretagne* (AniDyn-MT grant) and the European Molecular Biology Organization.

Author contributions

Conceptualization, JP, HB, and MD; Methodology, HB, LC, and JP; Software, JP and HB; Validation / Formal Analysis, HB, SP, and LC; Investigations / Data Curation, HB, SP, LC, and JP; Writing – Original Draft, HB and JP; Writing - Review & Editing, HB, LC, MD, and JP; Supervision, JP.

Competing financial interests

No competing financial interests.

bioRxiv preprint doi: https://doi.org/10.1101/103937; this version posted April 5, 2017. The copyright holder for this preprint (which was not certified by peer review) is the author/funder. All rights reserved. No reuse allowed without permission.

Figures

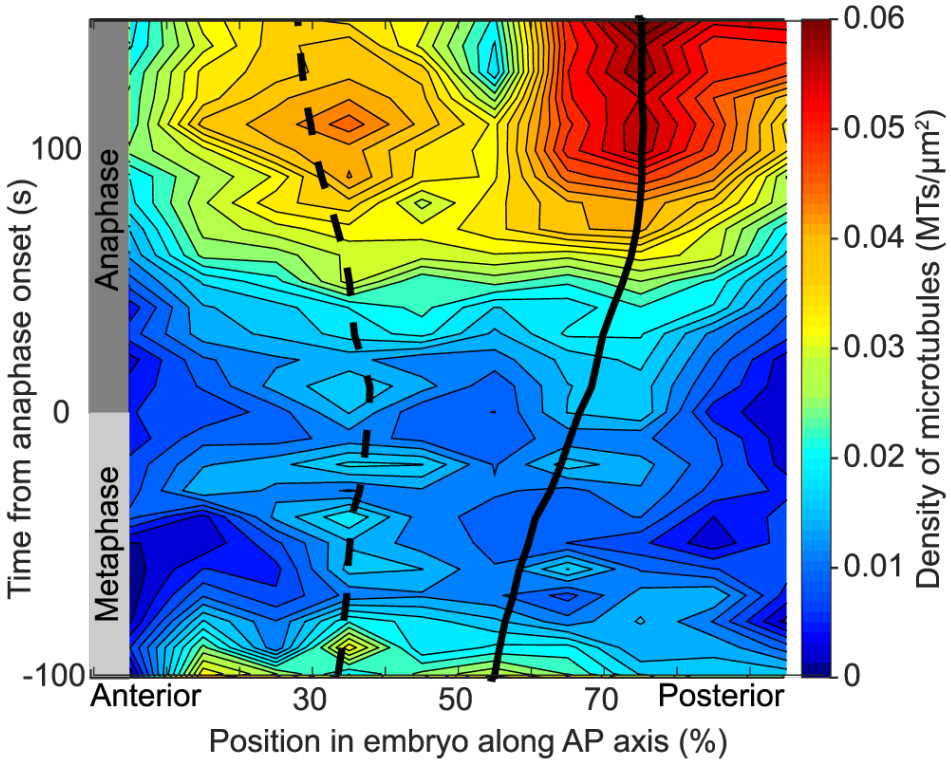

Figure 1: Microtubule contact density at the cell cortex in *Caenorhabditis elegans.* Microtubule contact density at the cortex obtained by spinning disk microscopy, and viewing a YFP::α-tubulin strain (see Methods). The densities were averaged along the AP axis (in 10 regions of equal width) and across time (10 s running window), shown here as a heat map (*N* = 22 *C. elegans* embryos). The trajectories of the centrosomes obtained by imaging the same strain in the spindle plane were superimposed (*N* = 8). The dashed line represents the anterior centrosome trajectory, and the solid line indicates the posterior one.

bioRxiv preprint doi: https://doi.org/10.1101/103937; this version posted April 5, 2017. The copyright holder for this preprint (which was not certified by peer review) is the author/funder. All rights reserved. No reuse allowed without permission.

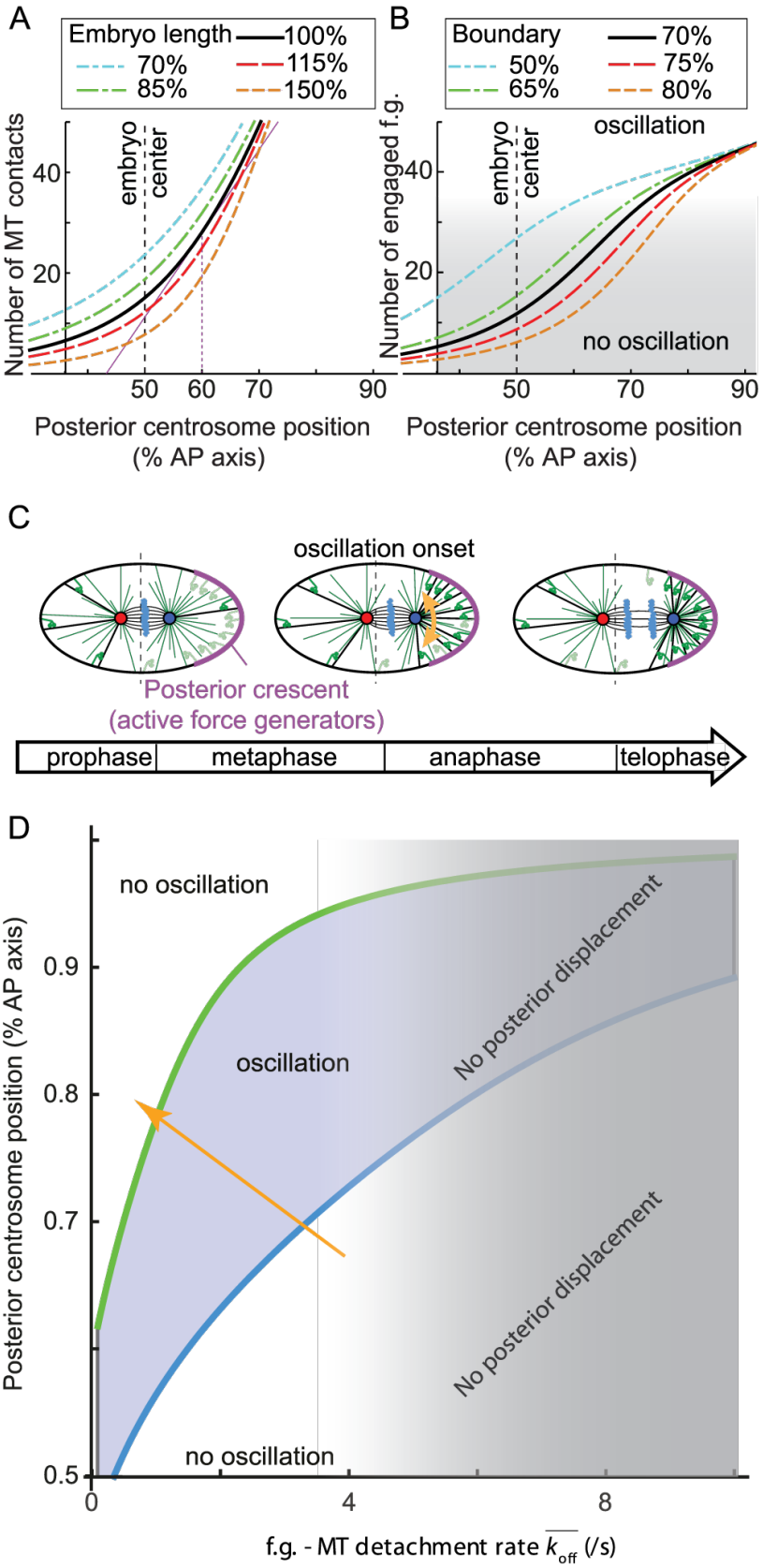

Figure 2: Expanded "tug-of-war" model of pulling force regulation and spindle oscillations. (**A**) Modelled number of microtubules (MTs) contacting the cortex in the active region having a boundary at 70% of the current anteroposterior (AP) axis versus the posterior displacement of the centrosome along that axis. The embryo length varies from 70

bioRxiv preprint doi: https://doi.org/10.1101/103937; this version posted April 5, 2017. The copyright holder for this preprint (which was not certified by peer review) is the author/funder. All rights reserved. No reuse allowed without permission.

to 150% of the length of the untreated one (Supplementary Text 2.1.3). For the untreated embryo (thick black line), when the centrosome position was above 60%, the number of contacts started to increase steeply (purple line). (**B**) Number of engaged force generators versus the posterior displacement of the centrosome along the AP axis, with the active region boundary expressed as a percentage of embryo length (Supplementary Text 2.2.2). The thick black line represents a boundary at 70%, mimicking the untreated embryo. In this case, when the centrosome reached 60% of the AP axis, the number of engaged force generators increased steeply and saturated above 70%, causing a switch-like behavior. Blue and green curves show *let-99(RNAi)* experiments where the boundary was displaced anteriorly. Red and orange curves show cases of posteriorly displaced boundaries. Gray shading indicates when the number of engaged force generators was too low to permit oscillation (below threshold). (**C**) Expanded tug-of-war schematic representation. At early metaphase, the spindle is roughly centered (*left*); around anaphase onset, it reaches 70% of the AP axis and starts oscillating (*middle,* orange arrow); and after anaphase, it reaches its final position, about 80% of AP axis (*right*). The anterior and posterior centrosomes are red and blue disks, respectively, and the chromosomes are light blue clouds. Microtubules that emanate from the centrosomes will either reach the cortex and find an active force generator (thick black lines), or reach an inactive region of the cortex or be too short to reach the cortex (thin green lines). The posterior crescent containing the active force generators is purple, and inactive and engaged (i.e. active) force generators are light and dark green, respectively. Within the spindle, microtubules are represented by thin black lines. A vertical dashed line marks the middle of the AP axis. **(D)** Stability diagram of the expanded model as a function of the detachment rate (off-rate $\overline{k_{off}}$, inverse of the processivity, *x*-axis) and of the position of the centrosome as a percentage of embryo length (*y*-axis). The unstable region (blue) corresponds to the values of off-rate and posterior-centrosomal position enabling oscillation development (Supplementary Text 2.2.5). The critical values are marked by the thick blue and green lines. The orange arrow indicates the typical phase trajectory during mitosis based on the parameters used in this study. The greyed-out area shows that above a detachment rate threshold, the posterior displacement of the spindle/posterior centrosome no longer occurs (orange curve in Figure 5). The centrosome needs to reach a position that is posterior enough to enable oscillations while force generators display a realistic processivity (measured to 1-2 s^{-1} in metaphase[13]). Furthermore, the sloping blue line corresponding to oscillation onset suggests that it is controlled by both position and processivity. In contrast, the steep green return-to-stability line, showing the oscillation die-down, suggests that this phenomenon depends mostly on processivity. For all plots, the parameters used are listed in Supplementary Text 4.

bioRxiv preprint doi: https://doi.org/10.1101/103937; this version posted April 5, 2017. The copyright holder for this preprint (which was not certified by peer review) is the author/funder. All rights reserved. No reuse allowed without permission.

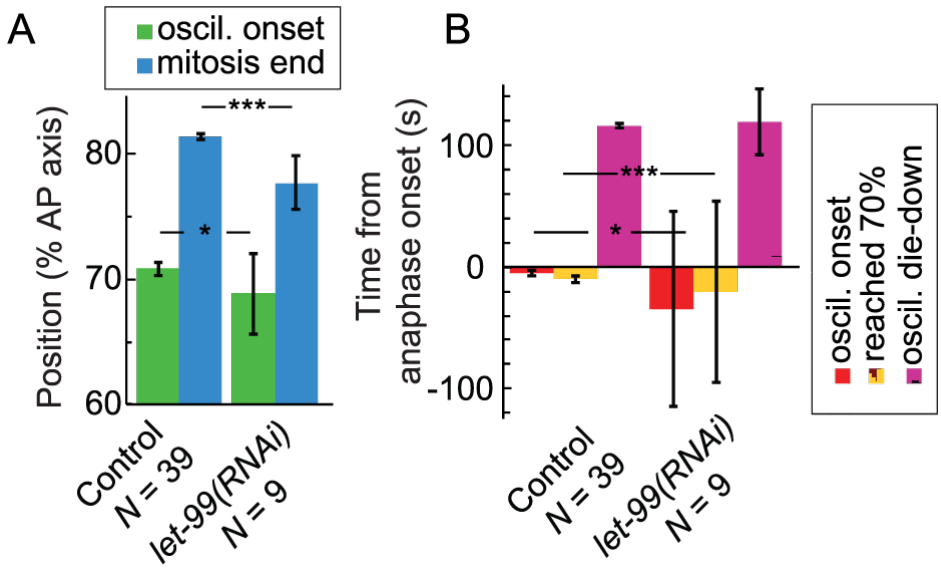

Figure 3: Force generator locations contribute to setting the positional switch on cortical pulling forces. (A) Positions of the posterior centrosome at oscillation onset and die-down. **(B)** Timings of oscillation onset, die-down, and their arrival at 70% of embryo length when the size of the active region is changed. We measured *let-99(RNAi)* (*N* = 9) and untreated (*N* = 39) embryos at 23ºC, with centrosomes labelled by GFP::γ-tubulin. Error bars indicate SD, and asterisks indicate significant differences (see Methods).

bioRxiv preprint doi: https://doi.org/10.1101/103937; this version posted April 5, 2017. The copyright holder for this preprint (which was not certified by peer review) is the author/funder. All rights reserved. No reuse allowed without permission.

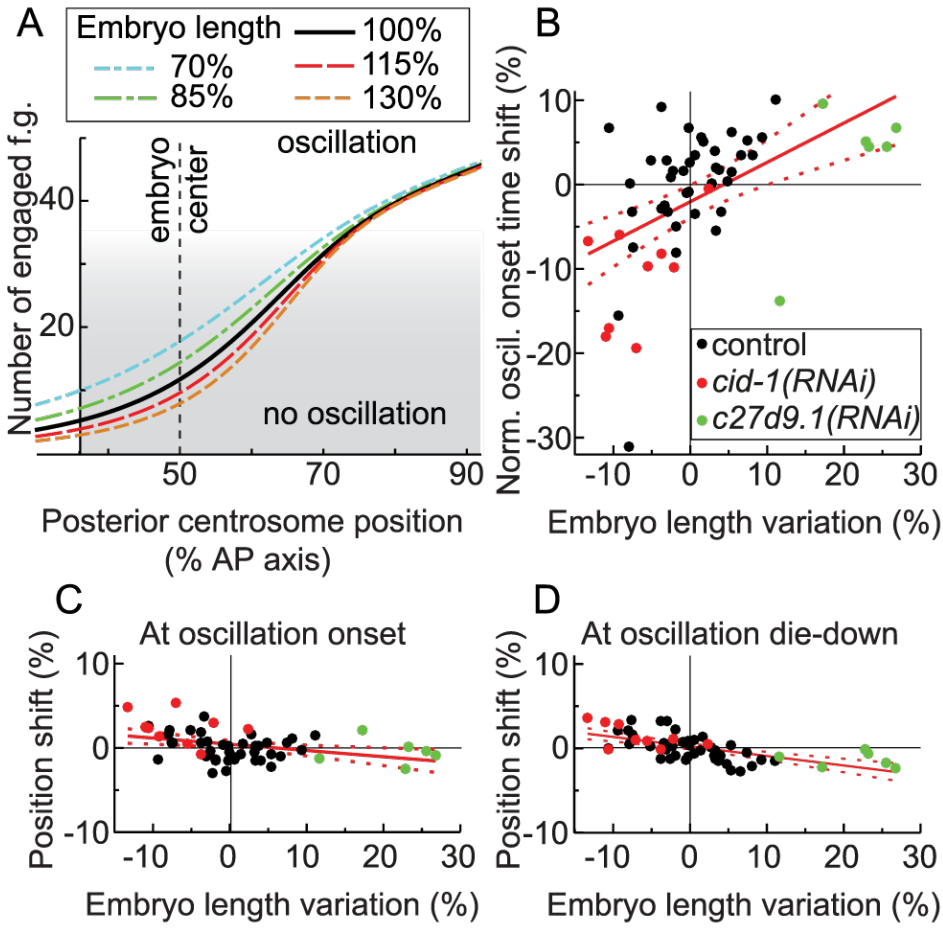

Figure 4: Embryo length has less effect on oscillation onset and die-down positions than on their timing. (A) Modelled number of microtubules contacting the active region of the cortex *versus* the posterior displacement of the centrosome along the AP axis as a percentage of embryo length. The line colours indicate the embryo length: untreated embryos are black; the shorter embryos produced by *cid-1(RNAi)* are blue and green; and the longer ones from *c27d9.1(RNAi)* are red and orange. The parameters used are listed in Supplementary Text 4. Grey shading indicates when the number of engaged force generators was too low to permit oscillation (below threshold). **(B-D)** Variations in embryo lengths as compared to the control (normalized by the average length, see Supplementary Experimental Procedures) are shown here versus the (B) shift in oscillation onset normalized by the control's average pro-metaphase and metaphase duration; and versus the (C) oscillation onset and (D) die-down positions as compared to the control. The solid red lines indicate the linear least square fits, with slopes of 0.47 ± 0.11 ($p = 5 \times 10^{-5}$ compared to null slope), -0.07 ± 0.02 ($p = 0.005$) and -0.11 ± 0.02 ($p = 2.6 \times 10^{-7}$), respectively. The red dashed line is the standard error of the mean. We measured $N = 9$ *cid-1(RNAi)*, $N = 6$ *c27d9.1(RNAi),* and $N = 39$ untreated embryos with GFP::γ-tubulin-labelled centrosomes at 23ºC. The control embryos used are the same as shown in Figure 3. Dots indicate individual embryos, and the average control values (0 shift) are thin black lines.

bioRxiv preprint doi: https://doi.org/10.1101/103937; this version posted April 5, 2017. The copyright holder for this preprint (which was not certified by peer review) is the author/funder. All rights reserved. No reuse allowed without permission.

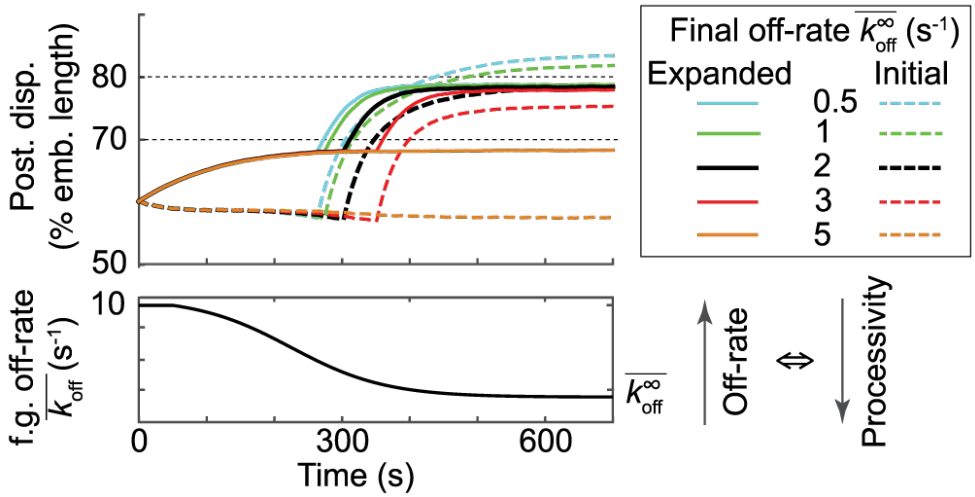

Figure 5: The expanded model of pulling force regulation offers resistance to final force generator processivity variations. Color-coded stochastic simulations of the displacement of the posterior centrosome when varying the final force generator (f.g.) detachment rate (off-rate, the inverse of the processivity). The dashed lines indicate the results from the initial model, and the solid lines are from the expanded one (Supplementary Text 3). A typical example of f.g. off-rate evolution throughout mitosis is shown at the bottom. Earlier than 300 s, whatever their final values are, detachment rates are very close, leading to superimposed posterior centrosome trajectories. The dispersion of the final values from the initial model revealed a lack of robustness to variations in the final off-rate that disappeared in the expanded model. The parameters used are listed in Supplementary Text 4.

bioRxiv preprint doi: https://doi.org/10.1101/103937; this version posted April 5, 2017. The copyright holder for this preprint (which was not certified by peer review) is the author/funder. All rights reserved. No reuse allowed without permission.

Table

Characteristic measured (mean ± s.e.m.)	control (*N* = 17)	*such-1(h1960)* (*N* = 15)
Oscillation onset *T1* (s)	-11.03 ± 5.50	-39.83 ± 5.93 $p = 9 \times 10^{-4}$
Posterior centrosome (CS) reaching 70% of AP axis *T2* (s)	-11.76 ± 5.68	-85.50 ± 17.15 $p = 6 \times 10^{-4}$
From oscillation onset to post. CS reaching 70% *T1* - *T2* (s)	0.74 ± 4.96	45.67 ± 15.82 $p = 0.015$
Maximum oscillation amplitude (posterior) (%)	20.78 ± 0.65	22.71 ± 0.61 $p = 0.035$
Nuclear envelope breakdown time (s)	- 164.84 ± 3.48	- 291.04 ± 5.40 $p = 1 \times 10^{-17}$
Oscillation die-down *T3* (s)	124.4 ± 7.0	117.5 ± 7.63 $p = 0.507$
Oscillation duration *T3* - *T1* (s)	135.4 ± 8.9	157.3 ± 9.7 $p = 0.11$
Posterior centrosome position at oscillation onset (%)	70.68 ± 0.89	70.76 ± 0.49 $p = 0.936$
Posterior centrosome position at oscillation die-down (%)	79.51 ± 0.40	79.01 ± 0.69 $p = 0.515$
Embryo length (µm)	52.60 ± 0.86	53.98 ± 0.80 $p = 0.237$
Embryo width (µm)	35.21 ± 0.61	33.25 ± 0.53 $p = 0.019$

Table 1: Timing and position of metaphase and anaphase events in untreated embryos and in delayed-anaphase mutants. Embryos labelled with SPD-2^{CEP192}::GFP;HIS-58^{H2B}::mcherry were viewed at 18°C, and spindle poles tracked. We compared untreated embryos with an ANAPC5 homolog mutant, the *such-1(h1960)* whose gene codes for an APC/C[32]. Times were measured from the onset of anaphase, and the peak-to-peak oscillation amplitude is shown as a percentage of embryo width. Positions along the AP axis are shown as a percentage of embryo length. Error bars indicate the standard error of the mean. *p* values are reported for Student's *t*-test.